Impact of Reservoir Permeability, Permeability Anisotropy and Designed Injection Rate on CO2 Gas Behavior in the Shallow Saline Aquifer at the CaMI Field Research Station, Brooks, Alberta

Yu, X., Ahmadinia, M., Shariatipour, S. M., Lawton, D., Osadetz, K. & Saeedfar, A.

Original citation & hyperlink:
Yu, X, Ahmadinia, M, Shariatipour, SM, Lawton, D, Osadetz, K & Saeedfar, A 2020, 'Impact of Reservoir Permeability, Permeability Anisotropy and Designed Injection Rate on CO2 Gas Behavior in the Shallow Saline Aquifer at the CaMI Field Research Station, Brooks, Alberta', Natural Resources Research, vol. 29, no. 4, pp. 2735–2752.
https://doi.org/10.1007/s11053-019-09604-3

DOI 10.1007/s11053-019-09604-3
ISSN 1520-7439
ESSN 1573-8981

Publisher: Springer

The final publication is available at Springer via http://dx.doi.org/10.1007/s11053-019-09604-3

Impact of reservoir permeability, permeability anisotropy and designed injection rate on CO_2 gas behaviour in the shallow saline aquifer at the CaMI Field Research Station, Brooks, Alberta

Xinran Yu[1], Masoud Ahmadinia[2,*], Seyed M. Shariatipour[2], Don Lawton[1,3], Kirk Osadetz[3] and Amin Saeedfar[3]

[1] University of Calgary, Calgary, CANADA
[2] Centre for Fluid and Complex Systems, Coventry University, UK
[3] Containment and Monitoring Institute, Calgary, CANADA

[*]Correspondence: Ahmadinm@uni.coventry.ac.uk

Abstract

Carbon capture and storage (CCS) is part of Canada's climate change action plan to reduce greenhouse gas (GHG) emissions. The Containment and Monitoring Institute Field Research Station (FRS) contributes to scientific and technological progress that ensures the secure underground storage of CO_2. In this study, the process of shallow CO_2 gas injection (300 m) and subsequent plume development at the FRS is investigated using numerical simulation. Due to reservoir uncertainties, various sensitivity analyses are performed to illustrate their effects on CO_2 saturation, plume distribution and CO_2 dissolution in a saline reservoir in response to variations in horizontal permeability (k_h), k_v/k_h ratio and CO_2 injection rate. The distance of horizontal migration of the plume post-injection is predicted analytically and the result is validated against the numerical simulation prediction.

Results show that increases in k_v/k_h ratio result in increases in both vertical and lateral plume migration and decreases in dissolution rate and CO_2 solubility. It is also indicated that the subsequent post-injection CO_2 migration rate is independent of both k_v/k_h and previous injection rate. Dissolution varies significantly with changes in horizontal permeability. The model shows that increased horizontal permeability facilitates plume migration vertically and horizontally. Modeled permeability variations in horizontal permeability (k_h), k_v/k_h ratio have a progressively decreasing effect on plume vertical migration with time, while lateral migration effects increase with time.

Keywords: Case Study; Carbon Capture and Storage; CaMI Field Research Station; k_v/k_h ratio.

1. Introduction

Carbon Capture and Storage (CCS) plays an important role in mitigating climate change, as it provides a means of capturing and safely storing carbon from industrial emissions in subsurface geological media (UNCCS 2015). Both capture and storage in geological media must be performed efficiently to minimize CCS economic costs and energy requirements. Storage in geological media must be safe and secure to ensure public acceptance and safety and avoid contamination of other resources such as potable groundwater (IEA 2013). Currently, CCS is focused strongly on pore space storage in geological formations, predominately sandstones, due to their apparent lower economic costs and energetics (Metz 2005).

Subsequent to injection, the sequestered free CO_2 phase has the potential to migrate upwards due to buoyancy (a result of its low density) or to be influenced by hydrogeological mechanisms, such as regional formation water flow (Juanes et al. 2010). Buoyant motions are inhibited by storage complex cap rock lithological and permeability characteristics, while lateral migration is inhibited by lateral permeability variations due to storage complex structure and rock body stratification, in ways identical to petroleum entrapment, which is effective on timescales approaching 100 million years. However, storage complex containment risks are all positive and finite, due to uncertainties in both storage complex geological characterization and geomechanical changes induced, more likely during injection interval, but persisting into the post-injection interval. The security of the storage process is a priority that cannot be assured by its pre-injection characterization, that must be assured by continuous monitoring both during and subsequent to the injection interval (Bachu 2008; Carroll et al. 2009; Morris et al. 2011; Rutqvist et al. 2007). To avoid CO_2 escaping the storage complex site, the plume migration is of great importance to track and assess during injection and post-injection intervals.

The potential effects of storage complex pressure changes, as a function of storage complex permeability and porosity during and subsequent to the injection interval, can limit both storage complex capacity and injection rate (Birkholzer et al. 2015). The subsurface pressure effects extend beyond the physical limits of the plume of injected fluid and, although pressure interference is typically not permitted, this can impact other subsurface activities and wells – both withdrawals and introductions - typically, but not exclusively, in the storage formation (Birkholzer and Zhou 2009). Therefore, storage complex pressure management is critically significant for project regulatory compliance. Additional subsurface interventions have been proposed to manage subsurface pressure impacts while improving storage project performance such as, brine production, both active or passive may improve project performance, increasing both higher storage capacity and injectivity in the storage complex (Bergmo et al. 2011; Birkholzer et al. 2012; Buscheck et al. 2012; Cihan et al. 2015; Dempsey et al. 2014).

Compliance with typical regulatory requirements for permission to inject and store in subsurface pore space typically requires a model of the proposed injection program performed in consideration of the geostatic model at the proposed storage complex site (Tucker et al. 2016). In practice, it is necessary to monitor the project to demonstrate the containment of the injected fluid in the storage complex. It is also important to show that project performance conforms with the reservoir models for eventual project regulatory approval, risk assessment and liability transfer (Rock et al. 2017). Some monitoring technologies have been applied to the existing sites recently, such as 4D seismic and 4D gravity, by which CO_2 saturation and migration plume are successfully detected (Arts et al. 2004; Daley et al. 2007).

In addition to these monitoring technologies, some research work has been conducted to investigate the impacts of some geological properties on the behaviour and vertical and horizontal movement of CO_2 plume (Ahmadinia et al. 2019; Bryant et al. 2006; Doughty 2010; Flett et al. 2007; Hesse and Woods 2010; Hovorka et al. 2004; B. Li and Benson 2015; Shariatipour, Pickup, et al. 2016a, 2016b; Taku Ide et al. 2007; Zhou et al. 2010). The influence of small-scale heterogeneities on upward CO_2 plume migration is studied by Onoja and Shariatipour (2019) and B. Li and Benson (2015), and they find that ignoring small-scale heterogeneities can result in an overestimation of the migration speed. Sensitivity studies conducted by Doughty (2010) indicate that some model parameters including permeability, permeability anisotropy and the maximum residual gas saturation also strongly affect the extent of CO_2 plume movement. Some scholars have also investigated the impact of the permeability anisotropy (k_v/k_h) by using three k_v/k_h values (0.01, 0.1 & 1) and found out that k_v/k_h is a very influential factor on plume migration and CO_2 dissolution during the CO_2 injection into the storage formations (Shariatipour, Mackay, et al. 2016). Additionally, capillary pressure plays an important role in CO_2 migration (Onoja et al. 2019; Zhou et al. 2010). Al-Khdheeawi et al. (2017) demonstrate that reservoir wettability and heterogeneity both have impacts on CO_2 plume migration: a higher CO_2 wettability in the reservoirs helps with CO_2 vertical migration while a water-wet reservoir always retains CO_2 movement; reservoir heterogeneity reduces the vertical migration and induces the lateral migration. Previous simulation works presented by Chasset et al. (2011) and Newell et al. (2019) show that stratigraphic uncertainty is also an important factor of the upward progression of the injected CO_2. Therefore, it is significant to characterize the reservoir properties and constrain these parameters prior to CO_2 injection (Doughty 2010).

The FRS is designed primarily as a facility to demonstrate and develop monitoring technologies (Lawton et al. 2019). It attempts to identify a simulated containment failure in the hypothetical underlying storage complex, while ensuring the protection of the groundwater and surficial resources, facilities and environments (<225 m to surface). While shallow formations are not typically considered as efficient storage CO_2 sequestration reservoirs due to the low density of gas phase storage (Yang et al. 2014), they are commonly available and they might provide economical storage options, especially where low ground temperatures provide the opportunity for conversion to a methane clathrate, as in the Athabasca region of Alberta, or sub-permafrost settings (Zatsepina et al. 2014). As CO_2 is injected into a depleted methane reservoir, reservoir pressure initially rises to meet conditions for hydrate formation. As hydrate forms, the reservoir temperature increases following the equilibrium of the three-phase hydrate equilibrium. CO_2 fraction in the hydrate phase rises with injection time and methane can be displaced by injected CO_2 (Zatsepina et al. 2014).

1.1 Objective and Approach

The objective of this study is to model a potential CO_2 injection and plume development in a shallow saline aquifer in Upper Cretaceous sandstones at the FRS and to improve the characterization and understanding of CO_2 migration in a shallow formation, where gas-phase CO_2 interacts with pore space fluids as it moves away from the point of injection. The results of this study can be used to compare the actual plume migration in the storage site in the future during the injection phase and/or when surface and downhole monitoring data are available.

Various sensitivity analyses are performed to illustrate their impacts on CO_2 saturation, plume distribution and CO_2 dissolution using different horizontal permeability values, k_v/k_h ratio, and injection rate. Horizontal migration distance at the end of injection is calculated using numerical models and analytical methods and the results of both are compared. We also investigate the impact of caprock structure by comparing model plume migration in a layer-cake reservoir model compared to the actual structural reservoir model. In addition to evaluating monitoring technologies that can detect potential containment loss from a deep CO_2 storage complex into a shallow saline aquifer (300 m), the future comparison of our simulation outputs against the FRS monitoring and verification data will provide an improved understanding of injected gas migration processes and pathways in the shallow subsurface.

Although the FRS project looks primarily at the containment and monitoring of CO_2 storage especially from the perspective of monitoring, this ensures and detects threats to both the groundwater protection zone and surface environments. Additionally, the FRS provides us with an opportunity to consider gas-phase CO_2 storage and plume migration in a shallow saline aquifer, which may inform some novel CO_2 storage opportunities, such as shallow Athabasca region storage as a gas hydrate.

2. Methodology

2.1 Description of FRS

The FRS is located approximately 25 km southwest of Brooks, Alberta Canada (Figure 1), which is located on 200 hectares where both the surface and subsurface land are owned privately by Torxen Energy (Lawton et al. 2017).

The CO_2 injection well may operate at a rate of up to 1,000 tonnes per year (t/yr.). The injection experiment is designed to test the detection threshold of a variety of monitoring technologies (Lawton et al. 2017, 2019), but the consequential CO_2 injection program results in shallow pore space storage that is amenable to the analysis presented below. The shallow (~300 m) storage reservoir occurs in the Belly River Group, Oldman Formation basal shoreface sandstone. The injected CO_2 plume migration and pore water CO_2 concentration will be monitored, and its containment will be studied with an array of geophysical and geochemical monitoring tools deployed within three wells that penetrate the injection zone, as well with additional shallow geophysical technologies, water wells (<150 m deep) and approximately five dozen soil gas monitoring stations (Lawton et al. 2019). The Geo-model for this study is provided by CMC Research Institutes Inc (Lawton et al. 2017).

Figure 1. Location of the FRS.

2.2 Description of the geological model

Three vertical wells were drilled at the FRS (Lawton et al. 2017; Macquet et al. 2019). The injection well was drilled to 550 mKB (metres below Kelly Bushing) TD, through a succession of Upper Cretaceous strata that includes, in ascending stratigraphic order, Upper Colorado Group (predominantly shale with lesser sandstone (Medicine Hat Formation)), Lea Park Formation (predominantly siltstone and shale, with a few fine sandstones near the top), and Belly River Group (predominantly sandstones, siltstones, mudstones and coals). The wireline log interpretations from the three FRS wells are shown in Figure 2 (Lawton et al. 2017). The injection well is “plugged back” and completed to inject CO_2 into shoreface sandstones at the base of Belly River Gp. at about 300 mKB, which is the approximate TD of the two deepest monitoring wells (Figure 2) (Lawton et al. 2017; Macquet et al. 2019).

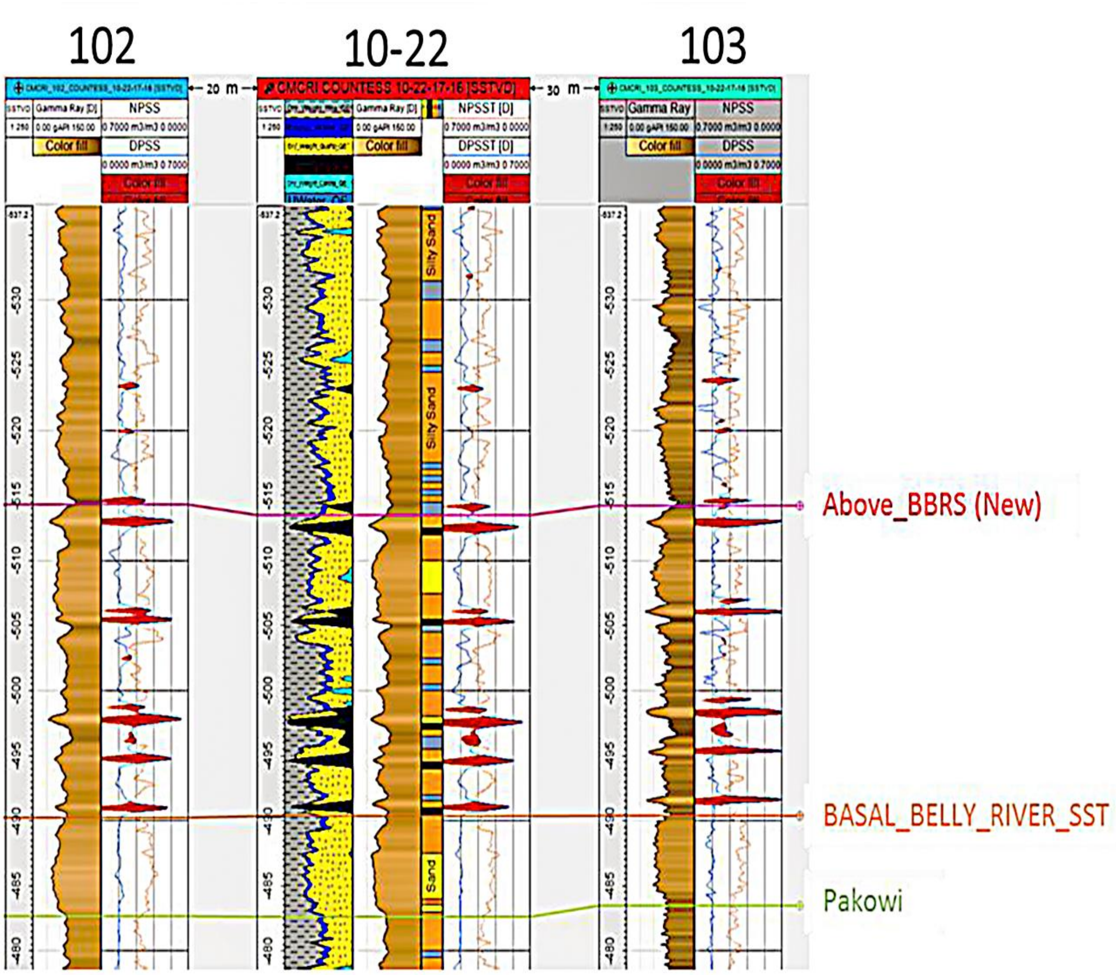

Figure 2. Interpretation of well logs from FRS. Well 102 is a geophysical observation well. Well 10-22 is the injection well and well 103 is a geochemical observation well (Lawton et al. 2017).

Additional details on the geological setting are discussed by Lawton et al. (2017). Currently injection occurs only into the basal Belly River sandstone at 300 mKB (Phase 1), although there is future potential to inject into the Medicine Hat Formation at 500 mKB (Phase 2) (Figure 3).

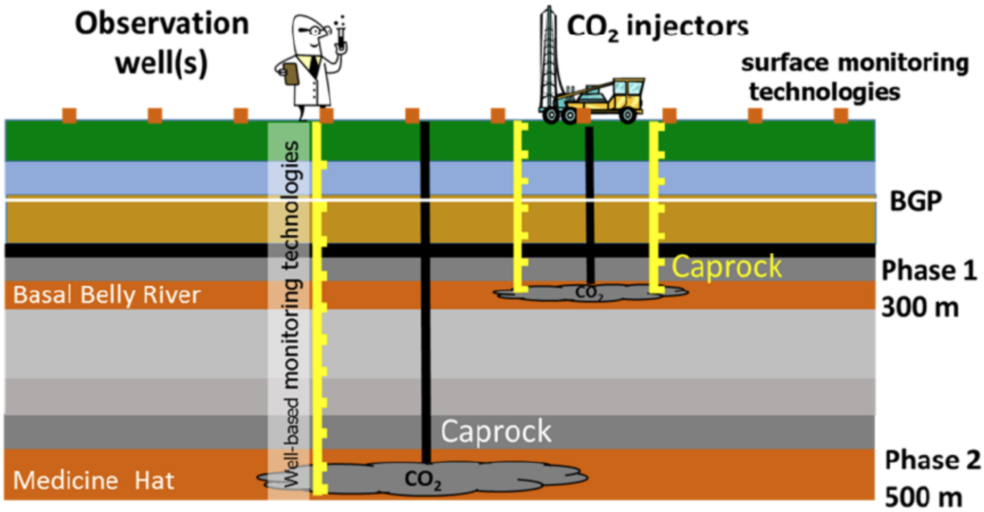

Figure 3. Schematic depth section of the Field Research Station (Phase 1: 300m, Phase 2: 500m) (Lawton et al. 2017).

The injection zone is predominantly saline water-saturated sandstones overlain by caprock shales and mixed sand/coal/shale successions (Lawton et al. 2017). In our simulation, the CO_2 injection rate is a constant 1,000 t/yr. for five years, with a cumulative 5000 t of CO_2 injected. The CO2STORE routine in Eclipse software is used for the simulation. Redlich-Kwong (RK) equation of state provides fluid properties. The solubility is calculated using previous work (Chang et al. 1996). The effect of salt and CO_2 on the water density is calculated using Ezrokhi's method (Zakirov et al. 2014).

Key reservoir model properties are listed in Table 1 (Dongas and Lawton 2016).

Table 1. Key reservoir properties at the FRS

Parameter	Value
Reservoir Dimensions (NX×NY×NZ)	124×124×73
Refined section Dimensions (NX×NY×NZ)	224×224×18
Cell size (X & Y) (m)	8
Total number of 3D grid cells	1122448
Rock compressibility (1/bars)	4.18 e-4
Porosity (mean) (%)	11
Permeability (mean) (mD)	0.57
Viscosity of water (Pa.s)	1.205 e-3
Viscosity of CO_2 (Pa.s)	1.49 e-5
Density of water (kg/m^3)	1000.74

Density of CO_2 (kg/m^3)	68.02
CO_2-water relative permeability	S_w=0.5, k_{rCO2}=0.5 k_{rwater}=0.00121
Salinity (ppm)	1000
k_v/k_h (base case)	0.1
Pressure at the 300 m depth (MPa)	2.944
Reservoir temperature (isothermal) (°C)	20
Annual Uniform Injection Rate (t/yr)	1,000
Base Case Injection Interval (yr.)	5
Simulation period (yr.)	15

Relative gas-water permeability curves are calculated using the widely accepted model based on capillary pressure data (K. Li and Horne 2006). The CO_2-water relative permeability end-point is calculated using the Brooks-Corey approximation (Brooks and Corey 1964). Figure 4 shows the model input relative permeability curves. The minimum water saturation and critical water saturation are set at 0.5. The maximum water saturation and the corresponding water relative permeability are set at 1. Except for CO_2 dissolution into water, geochemical compositional or phase changes are not considered, the maximum allowable BHP is 6.615 MPa, which is 90% of the calculated lithostatic pressure at the datum depth (300 mKB). In addition, some vertical and horizontal fractures are indicated from core measurements, but these are not included in the modeling. Remaining model uncertainties include reservoir pressure, fracture pressure, capillary pressure, vertical to horizontal permeability ratio, horizontal permeability and gas-water relative permeability. Additional model details are available (Dongas and Lawton 2016).

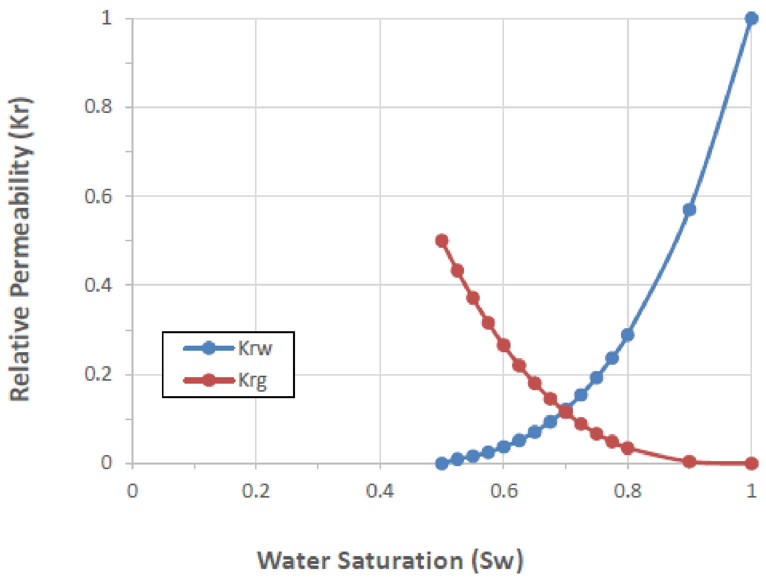

Figure 4. Relative permeability curve of CO_2/water (Dongas and Lawton 2016).

2.3 Sensitivity analysis set-up

We perform a sensitivity analysis to evaluate the impact of variations in horizontal permeability (k_h), vertical to horizontal permeability ratio (k_v/k_h), and injection rate on CO_2 saturation, the plume shape, and CO_2 dissolution. A few vertical and horizontal fractures are reported in the core analysis, most of them induced by the subsampling process and few of them observed in fresh slabbed cores, however, the presence of natural fractures cannot be precluded. At least three kilometres of sediments have been eroded since probably Mid-Eocene time, causing isostatic motions accompanying glacial loading and inter-glacial unloading. Although fracturing is not considered important, the variation in horizontal permeability and k_v/k_h can act as a rough attempt to simulate natural fractures, should they be present. Multipliers for injection rate are selected based on the regulation that BHP during injection does not exceed maximum allowable pressure that is a fraction of the lithostatic pressure. Different model scenarios are defined as shown in Table 2. For cases 2 and 3, vertical permeability is increased while horizontal permeability is kept constant. In cases 6 and 7, the injection period is decreased in correspondence to the rate, so the total injected CO_2 is the same as the base case. The modeled impacts of the caprock structure are also investigated by comparing the plume migration in the layered cake model to the observed structural model.

Table 2. Description of cases in the sensitivity analysis

Case #	Description
1	Base case, see Table 1.
2	As per Table 1 except, $k_v/k_h \times 5$
3	As per Table 1 except, $k_v/k_h \times 10$
4	As per Table 1 except, $k_h \times 0.1$
5	As per Table 1 except, $k_h \times 10$
6	As per Table 1 except, injection rate × 1.2 base case
7	As per Table 1 except, injection rate × 1.5 base case

2.4 Analytical solutions to migration distance

We employ an analytical method proposed by Nordbotten et al. (2005) to calculate plume migration distances from the injection well. This approach is only valid during the injection phase, during time intervals equivalent to the first five years of our numerical models. The analytical results are then compared to those of both homogeneous and heterogeneous reservoirs from numerical simulations. More details of how to calculate the CO_2 plume analytical solution can be found in Appendix.

3. Results and discussion

The saturation distributions and plume boundary at the end of the simulation for all the cases are shown in figures 5 (a) and 5 (b), respectively. Figure 5 (a) shows that increasing vertical permeability (cases 2 and 3) results in a thinner plume, which is due to the comparative ease of upward migration intrinsic to this model. Models show horizontal permeability has a major impact on the plume extent, as the CO_2 has migrated farthest and nethermost away from the injector, in cases 5 and 4, respectively. Compared to cases 2 and 3, the plume is thicker in case 5 than in the base case, which results in a better distribution of the plume throughout the aquifer, suggesting a higher dissolution rate. In addition, the results also show the migration distance is a weak function of the injection rate that is a consequence of model structure, specifically the limited injectivity due to low formation permeability combined with the fixed total injected volume for all the models (injection period is longer for cases with lower injection rates).

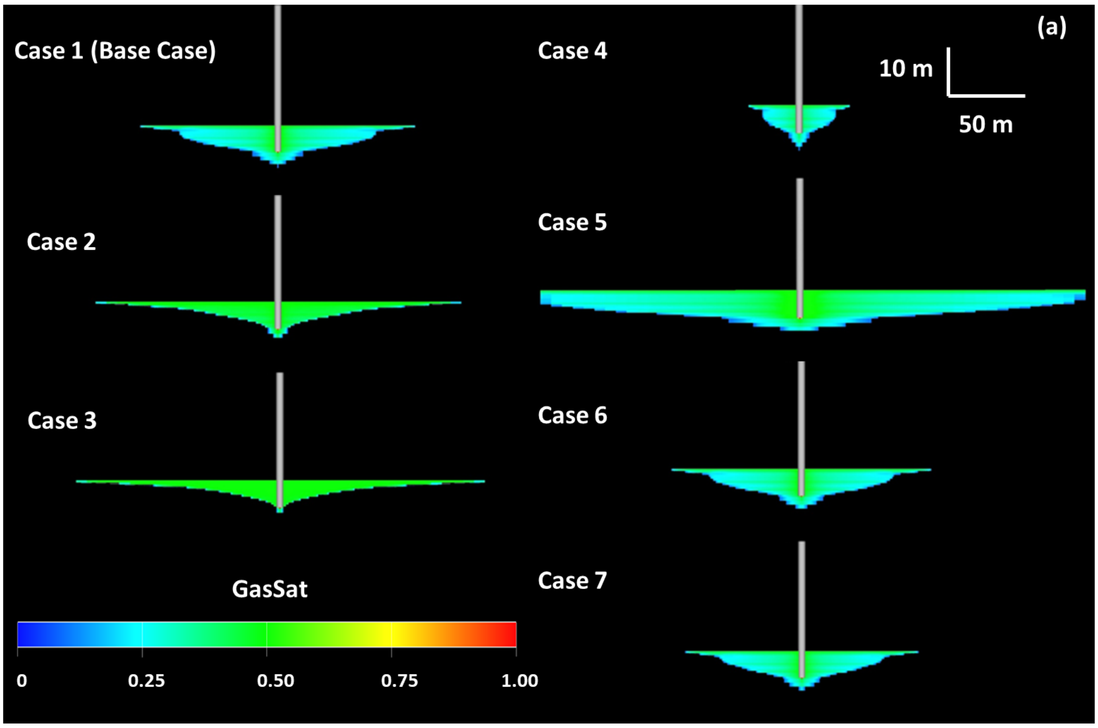
Case 1 (Base Case)
Case 2
Case 3
Case 4
Case 5
Case 6
Case 7
(a)
10 m
50 m
GasSat
0
0.25
0.50
0.75
1.00

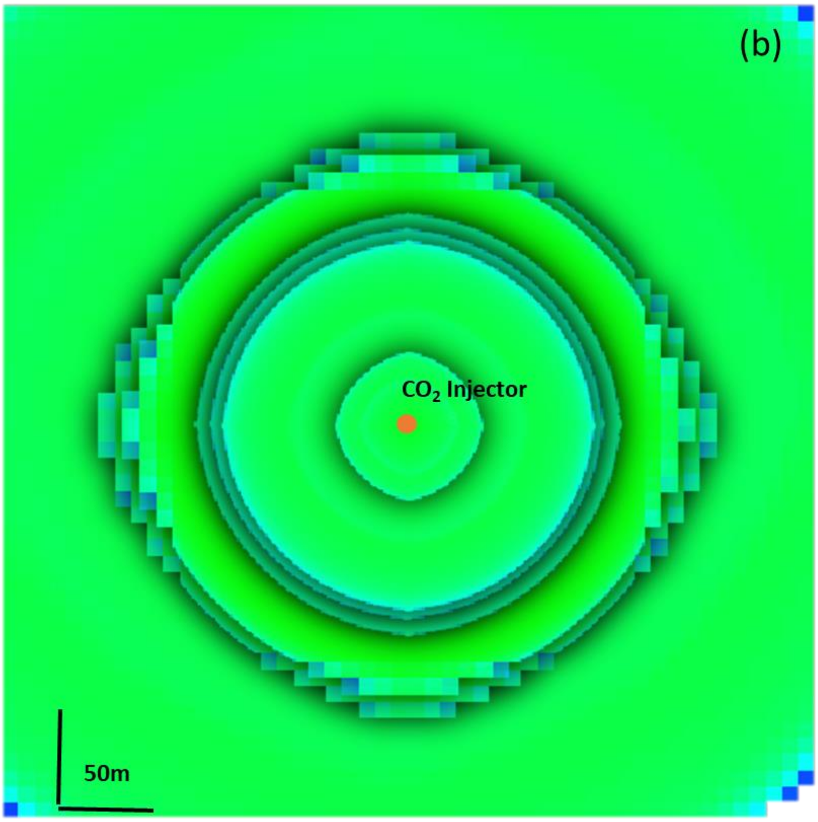
(b)
CO_2 Injector
50m

Figure 5. Stratigraphic distribution of various model CO_2 saturation in the injection zone pore space **(a)** and the horizontal extent of various model plume boundaries **(b)** at the end of the simulation (15 years). The horizontal limit of various model plume boundaries (Figure 5a) is shown for, sequentially cases 4 (smallest extent) through 7, 6, 1, 2, 3 and 5 (largest extent).

A summary of CO_2 plume horizontal migration distance and CO_2 saturation in the top layer for cases 1-7, at three time steps (1 month, 5 years, and 15 years) is shown in Table 3, and more details are discussed in Section 3.2.

Table 3. CO_2 plume horizontal migration distance and CO_2 saturation in the top layer for cases 1-7, at three time steps (1 month, 5 years, and 15 years).

Case #	**CO_2 plume horizontal migration distance (m)**			**CO_2 saturation in the top layer (%)**		
	1 month	**5 years**	**15 years**	**1 month**	**5 years**	**15 years**
1	7	74	103	0.31	0.49	0.5
2	7	87	133	0.31	0.49	0.5
3	7	96	145	0.35	0.5	0.51
4	1	20	34	0.07	0.39	0.44
5	23	107	149	0.42	0.5	0.51
6	7	72	95	0.32	0.48	0.49
7	7	68	86	0.31	0.49	0.49

In these simulations, the observation wells are located within 20 (well 1) and 30 metres (well 2) from the injector, respectively. Table 4 shows the time, saturation and layer at which the plume reaches each observation well. The times in Table 4 are a function of simulation time steps (one month). The cell saturation at the arrival time is provided. For example, the plume arrival time is the same for the base case and case 3, but the CO_2 saturation that plume reaches at the first observation well is higher for case 3.

The model injected CO_2 plume reaches the closer observation well #1, located to the southwest of the injector, first. The model CO_2 plume arrives at the observation wells in less than 3 months in all model cases except Case 4, in which the plume takes about 3 years to reach the observation well #1. In all cases, the CO_2 plume reaches observation wells first at model layer 11 but in cases 3 and 4, which have, respectively, the highest vertical permeability and lowest horizontal permeability the plume migrates to the observation well #2 first through model layer 1. In Case 3, this difference in the migration pathway is due to the increased vertical permeability that results in the CO_2 plume moving upwards faster compared to other models. In Case 3 most of the CO_2 reaches the top, or first, layer through which it laterally, subsequently. In Case 4, the decreased horizontal permeability produces similar migration effects as the CO_2 tends to migrate upward until it is redirected horizontally after contacting the model caprock barrier. Changing the injection rate has no significant effect on plume migration during the first few months of injection (see also section 3.1.3, below) resulting in similar migration histories base case, and cases 6 and 7. This could be due to the low permeability that regardless of the rate, allows a certain amount of fluid flow.

Table 4. Time, saturation and layer at which CO_2 plume reaches the observation wells

Case #	**1st observation well (20 m)**			**2nd observation well (30 m)**		
	Time to observe (days)	**Saturation**	**layer**	**Time to observe (days)**	**Saturation**	**layer**
1	91	0.19	11	151	0.07	11
2	91	0.17	11	181	0.14	11
3	91	0.13	11	181	0.14	1
4	1091	0.21	11	1821	0.22	1
5	31	0.23	11	31	0.27	11
6	91	0.19	11	151	0.07	11
7	91	0.19	11	151	0.07	11

Figure 6 shows the moment when the model CO_2 plume reaches observation wells 1 (6a) and 2 (6b). The results for horizontal and vertical migrations of the plume in all cases are discussed below. The horizontal migration distances of the CO_2 plume in the 1st model layer (left side of the well) which has slightly lower horizontal permeability than layer 11, is monitored at the FRS injection project. Model layers where horizontal and vertical migration are physically monitored at the FRS are shown by the dashed lines (Figure 6(b)).

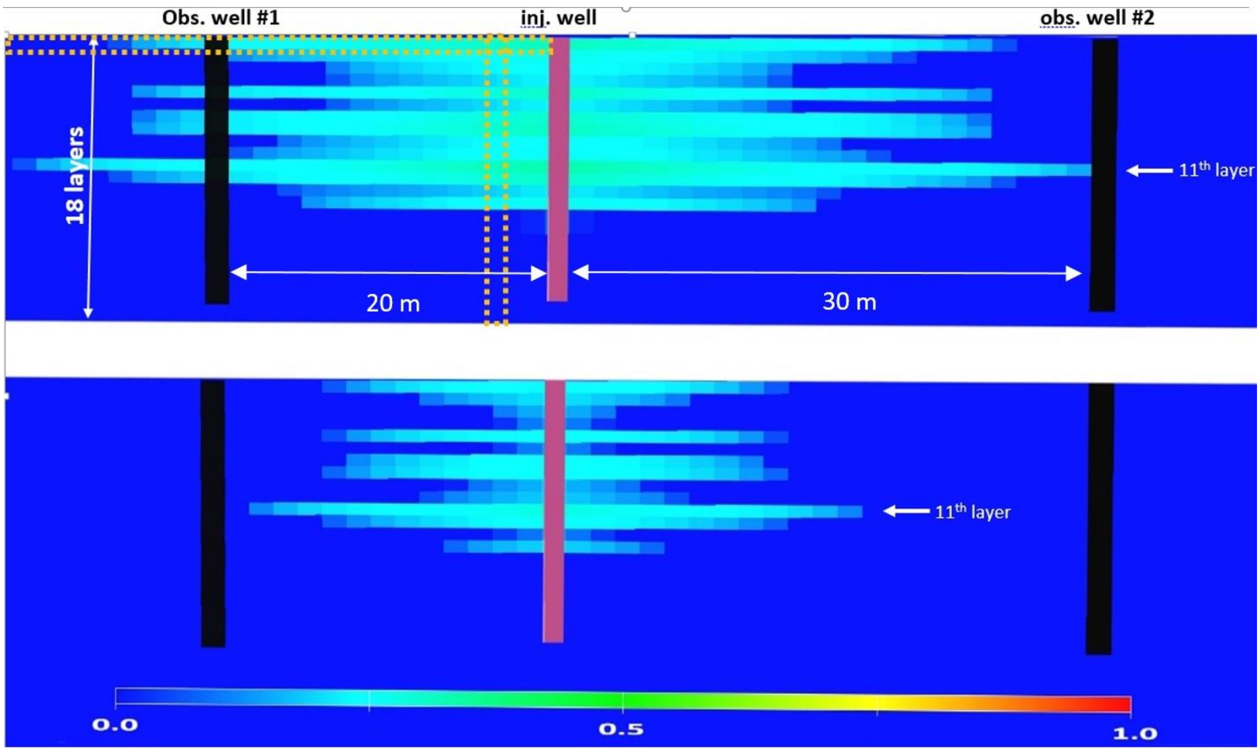

Figure 6. A cross-sectional view of CO_2 saturation distribution in the base case at the time of reaching observation wells #1(91 days after injection begins) and #2 (151 days after injection begins.

3.1 CO_2 saturation distribution

3.1.1 Vertical to horizontal permeability ratio (k_v/k_h)

The vertical to horizontal permeability ratio in the base case model is 0.1. This is increased to 0.5 and 1, in cases 2 and 3, respectively by increasing the vertical permeability only. In the base case, the CO_2 upwards migration is slower, which results in longer contact time with the pore space brine. Figure 7(a) shows CO_2 saturation along with the injectors versus vertical migration distance after one month, then five years and finally, 15 years for various (k_v/k_h) ratios of 0.1, 0.5 and 1, respectively. Vertical migration distance is defined by the distance between the top of the CO_2 plume and the lowest injection well perforation: zero-vertical migration coincides with the bottom of the perforations. As CO_2 migrates upwards, the vertical migration distance is positive and negative for portions of the plume below the lowest perforation. A small portion of the injected CO_2 migrates down to Pakowki Formation (below the Basal Belly River Group sandstone. One month after injection, the model CO_2 saturation distribution has a similar vertical trend in all three illustrated model cases (Figure 7). CO_2 also moves downward in cases 2 and 3 due to the higher k_v/k_h ratio. After five years, at the end of injection, more CO_2 has accumulated in the upper model layers of the case 3 model as compared to the base case and case 2 models. After fifteen years, at the end of the simulation, the CO_2 saturation in upper model layers increases to 0.5 in case 3, when the saturation below the lowest perforation is zero, which illustrates the expected roles of vertical permeability and buoyant forces. In both the base case and case 2, which have lower model vertical permeability the injected CO_2 is calculated to be trapped in the bottom model layers between 6.5 m and 4.0 m below the lowest perforation.

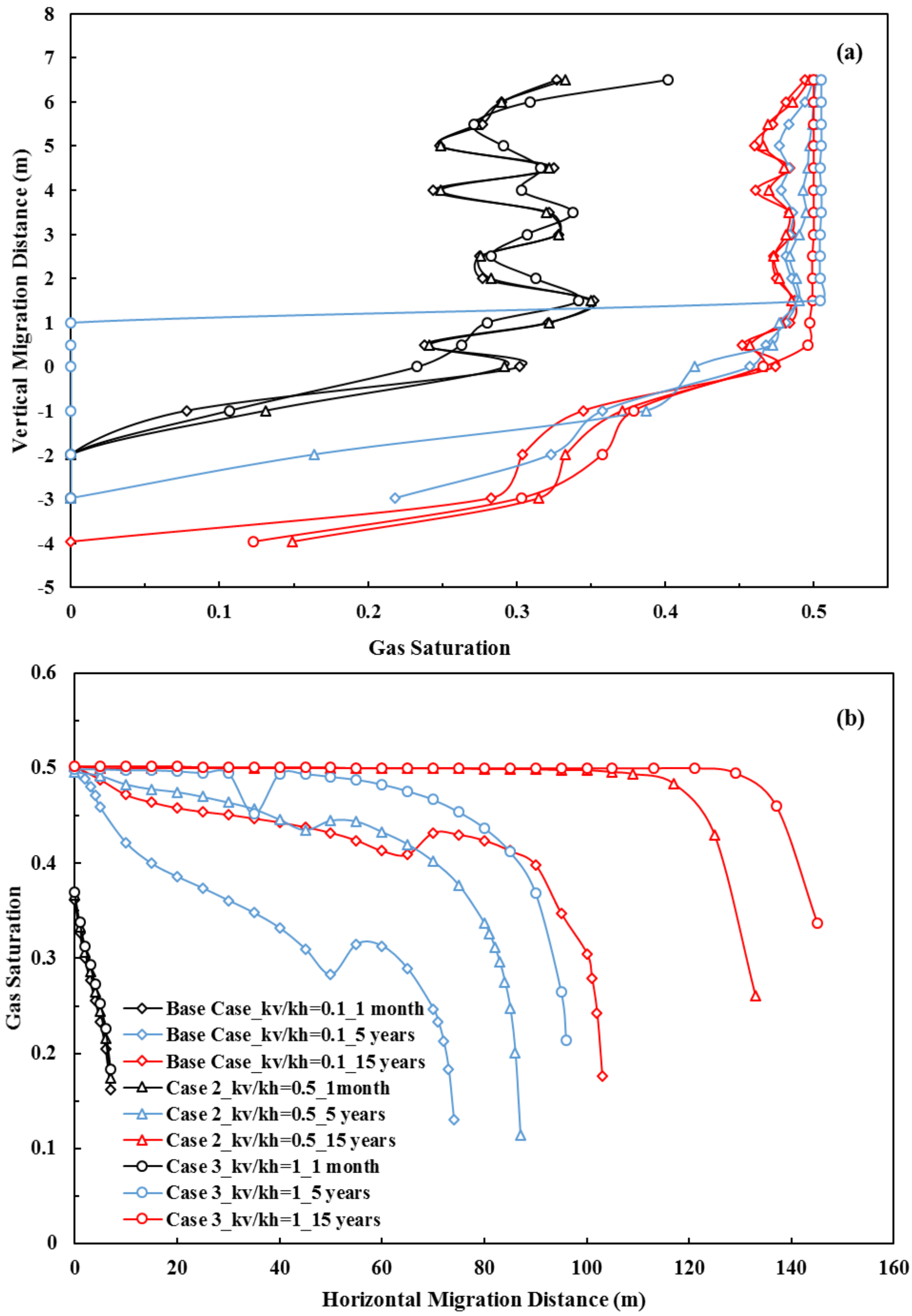

Figure 7. CO_2 saturation versus vertical **(a)** and horizontal **(b)** migration distances at the time steps of one month, five years, and 15 years, or the end of the simulation for model case 1-3 with various k_v/k_h ratios as explained in the legend of the figure.

Figure 7(b) illustrates CO_2 saturation as a function of horizontal migration distance at time steps of one month, five years and 15 years for (k_v/k_h) ratios of 0.1, 0.5 and 1. Zero horizontal migration coincides with the injector well. After one month, the model CO_2 plume has migrated about 7 m laterally in all three illustrated model cases while after five years, a higher k_v/k_h results in horizontal migration distances of 74 m, 87 m, and 96 m, for model cases 1-3 sequentially. Models predict that the CO_2 plume migrates vertically more quickly as k_v/k_h, increases, such that it reaches the caprock earlier than in model cases with lower k_v/k_h. In general, the sooner the plume contacts and is deflected horizontally by the caprock the longer the horizontal migration time, and the larger horizontal extent of the plume. The predicted lateral migration distance at the end of the simulation is highest for model case 3 at 145 m, followed by 133 m for model case 2 and smallest, or 103 m for the base case model.

The effect of k_v/k_h ratio on vertical and horizontal migration becomes more obviously manifest with time, and the higher the k_v/k_h ratio the larger the vertical and horizontal migration distances, typically. Moreover, higher k_v/k_h ratio models trap a larger proportion of the injected CO_2 in stratigraphically higher model layers. Doughty (2010) also finds that for a storage formation composed solely of sand, vertical anisotropy does play a dominant role in controlling upward migration.

3.1.2 Horizontal permeability

Base case horizontal permeability is multiplied by factors of 0.1 and 10 in model cases 4 and 5, respectively. Model results show that horizontal permeability plays an important role in vertical migration of the plume, as a result of the horizontal: vertical permeability anisotropy (Figure 8a). In case 4, the lowest horizontal permeability case, models predict that just a small portion of the injected CO_2 moved upwards and that its downward migration is negligible a month after injection begins. CO_2 saturation in upper model layers reached 0.3 and 0.4 in model cases 1 and 5, respectively. Except for case 4, the model plume is predicted to migrate downward. Five years after injection ends a small amount of CO_2 has migrated 4 m below the lowest perforation in all three cases. At the same point in time, the CO_2 saturation in upper model layers has increased to 0.36, 0.46 and 0.5 for cases 1, 4 and 5, respectively. A similar trend is predicted at the end of the simulation with slightly more CO_2 trapped in upper model layers (Figure 8).

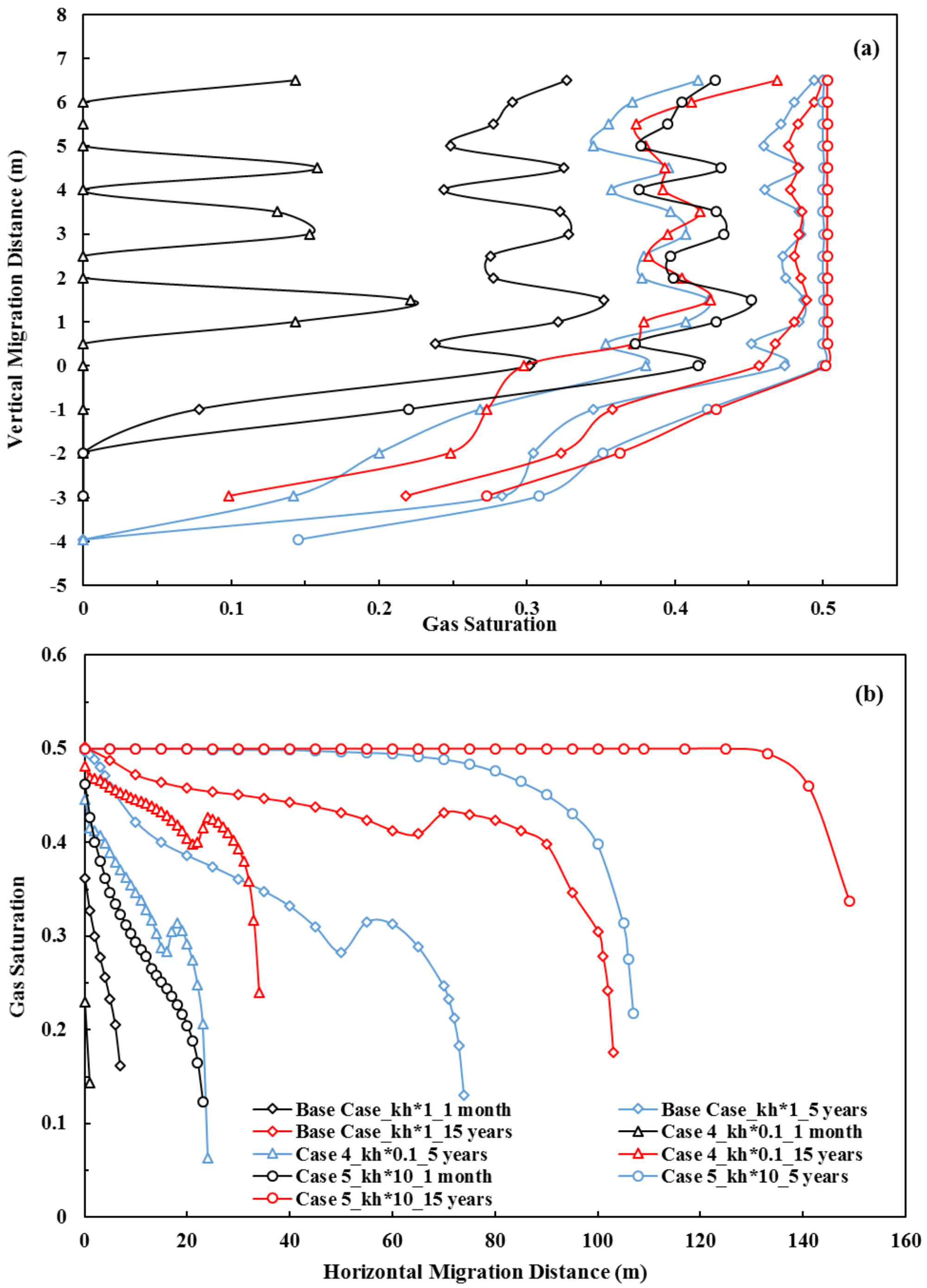

Figure 8. CO_2 saturation versus vertical **(a)** and horizontal **(b)** migration distances at time steps of 1 month, 5 years, and the end of the simulation (15 years), for three cases with different horizontal permeability.

Like the predicted vertical migration results, the horizontal migration distances are larger with higher horizontal model permeability (Figure 8b). Following one month of injection, the predicted horizontal migration distances are 1 m, 7 m, 23 m, for model cases 4, 1 and 5, respectively. After 5 years, the case 5 migration result is 107 m but only about 20 m for case 4, while in the base case the horizontal migration distance is as discussed above. The horizontal plume extends 34 m, 103 m and 149 m for cases 4, 1 and 5, respectively, at the end of the simulation. The previous study also confirms that higher horizontal permeability implies higher vertical permeability which enhances model plume vertical migration with decreasing effectiveness as the model progresses (Al-Khdheeawi et al. 2017; Doughty 2010; Han et al. 2010).

3.1.3 Injection rate

Injection rates are specified in m^3/day at standard conditions. The base case injection rate is 1600 sm^3/day, and this is increased by 20% to 1920 sm^3/day and 50% to 2400 sm^3/day in model cases 6 and 7, respectively. The total injected volume is constant in all model cases which implies shorter injection intervals for model cases 6 and 7. The simulation results indicate vertical migration distance is a weak function of the injection rate and that the plume’s upward movement is similar for all model cases due to the low vertical model permeability (Figure 9a).

In the first a few years, vertical and horizontal migration distances are, as a result, similar for all model cases, which is probably a consequence of the small injected volume and the resolution of the model. At the end of the simulation model, horizontal plume migration distances are 103 m, 95 m, and 86 m in model cases 1, 6 and 7, respectively. This suggests that injection at a lower rate over longer interval results in a more even distribution in the reservoir for given total injected volume of CO_2. Therefore, the variation of injection rate is seen to influence horizontal migration more strongly than vertical migration and that, for a given total injected volume, a lower injection rate results in a smaller maximum horizontal plume development. This has been reported by Yang et al. (2014) that the determination of an optimum injection rate is necessary to avoid the CO_2 leakage and improve storage efficiency in a shallow saline aquifer.

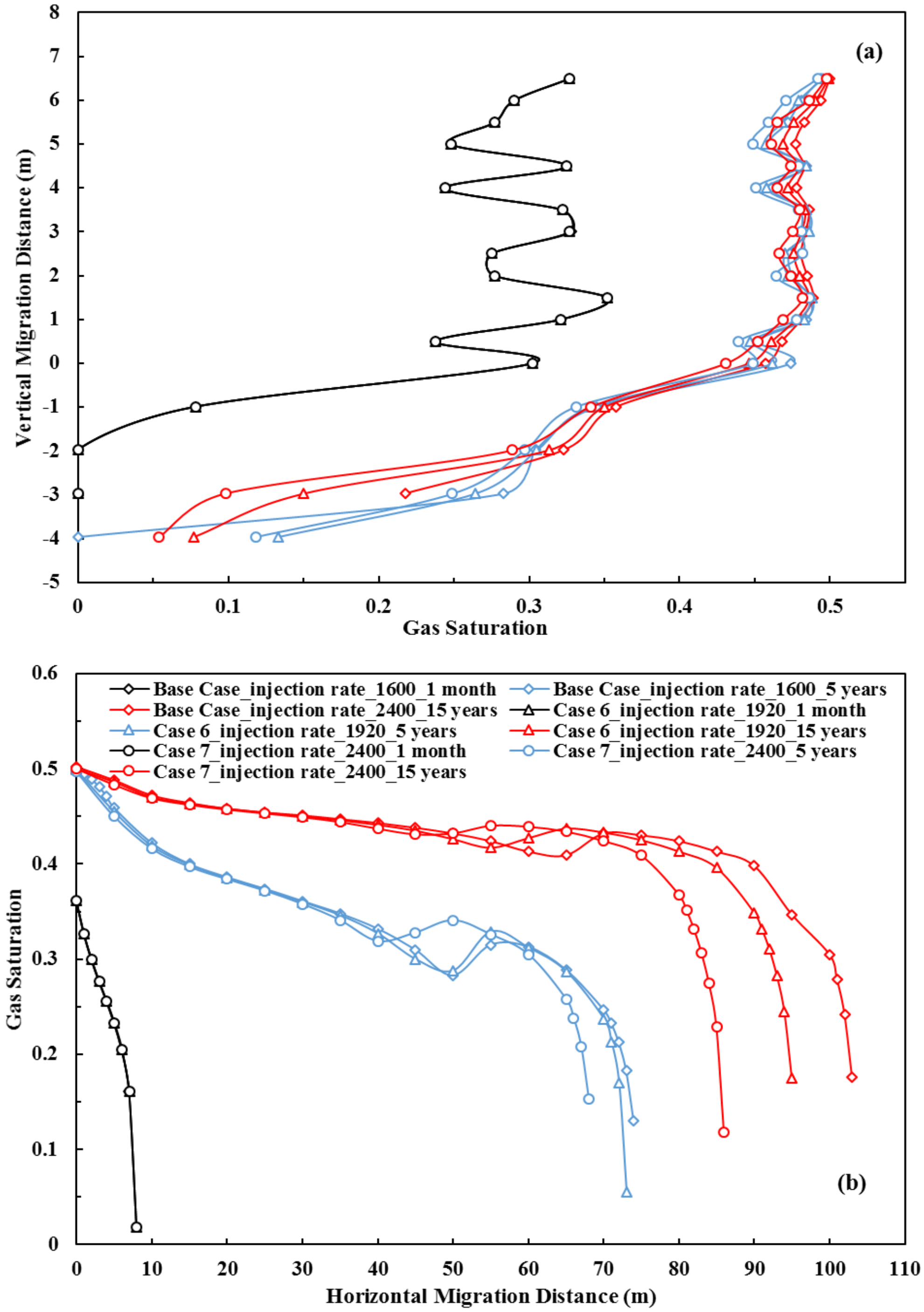

Figure 9. CO_2 saturation versus vertical **(a)** and horizontal **(b)** migration distances at the time steps of 1 month, 5 years, and the end of the simulation (15 years) for three cases with different injection rates.

3.2 Amount of CO_2 dissolved in brine

3.2.1 The k_v/k_h ratio

A higher k_v/k_h ratio, such as in model cases 2 and 3, results in lower predicted CO_2 dissolution. Figure 10 shows the cumulative amount of dissolved CO_2 in water (kg-mole) for all seven cases. The cumulative dissolution increases during the five years over which CO_2 is injected. The graph shows a similar dissolution trend in the early injection period (first two years) for all model cases except 4 and 5 that represent the extreme variations of model horizontal permeability. This suggests that model dissolution is not significantly dependent on k_v/k_h variations among model cases 1, 2 and 3. Subsequently, increased k_v/k_h ratios result in reduced model dissolution rates. During the post-injection period, the cumulative CO_2 dissolved in water is generally similar for model cases 1, 2 and 3, which are, respectively, 11 E+3, 9.65 E+3, and 9.15 E+3 kg-mole. Above we saw that higher k_v/k_h ratio results in a predicted faster upwards migration and a thinner model plume of a larger horizontal extent. Therefore, a higher k_v/k_h ratio results in a lower dissolution rate and total dissolved CO_2 for reasons not immediately apparent.

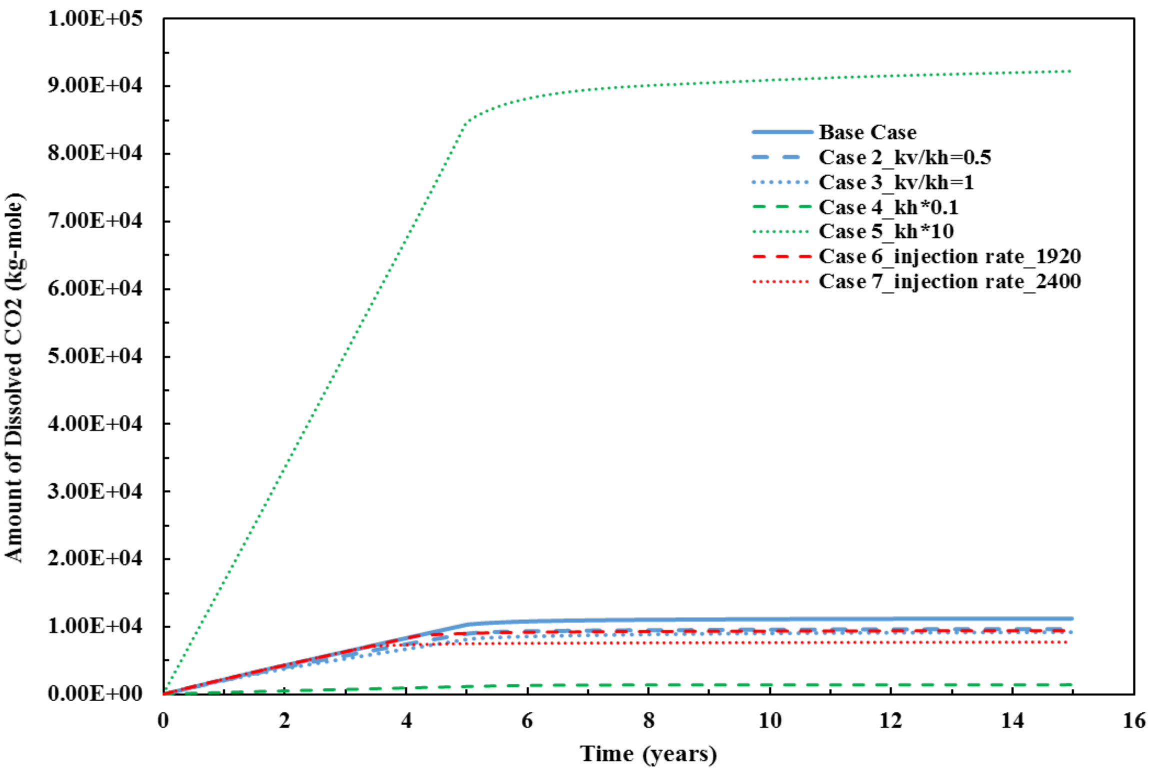

Figure 10. The amount of CO_2 dissolved in water versus time is shown for all model cases.

3.2.2 Horizontal permeability

Although other parameters are seen to have little or no impact on CO_2 dissolution in the early injection years, horizontal permeability significantly influences the rate and amount of dissolved CO_2 throughout the injection period (model cases 4 and 5 in Figure 10). During injection, an increase or decrease in horizontal permeability results in almost one order of magnitude increase or decrease in the amount of dissolved CO_2. The total amount of dissolved CO_2 at the end of the simulation is around 9.1E+4, 1.1E+4 and 1.45E+3 kg-mole for model cases 5, 1and 4, respectively. Moreover, while the dissolution remains constant for most model cases during the post-injection period, the results for case 5 predict a continuing increase rise that indicates the importance of horizontal permeability for dissolution rate.

3.2.3 Injection rate

Because of the constant total amount of injected CO_2, the amount of model CO_2 dissolved in the pore water varies with the model injection rate. For case 6 (1920 sm^3/day) the amount of dissolved CO_2 is 9440 kg-mole. However, the amount of dissolved CO_2 decreases in models with a higher injection rate. The amount of dissolved CO_2 is 7680 kg-mole for model case 7 (2400 sm^3/day). During the injection period, the total dissolved CO_2 is similar for model cases with similar permeability, independent of the injection rate. This suggests that higher injection rates result in a smaller plume that has less contact with fresh pore space brine (Figure 10).

3.3. Effect of storage complex structure

Storage complex structure especially that of the cap-rock, plays a significant role in plume migration direction and trapping efficiency. Here, we compare a flat, layered base case simulation (case 1) to a similar model that considers the real structural dip of model strata. When the model structure is considered, the injected free gas moves upwards below the caprock and much of the injected CO_2 becomes trapped in the small-scale structural trap (Figure 11).

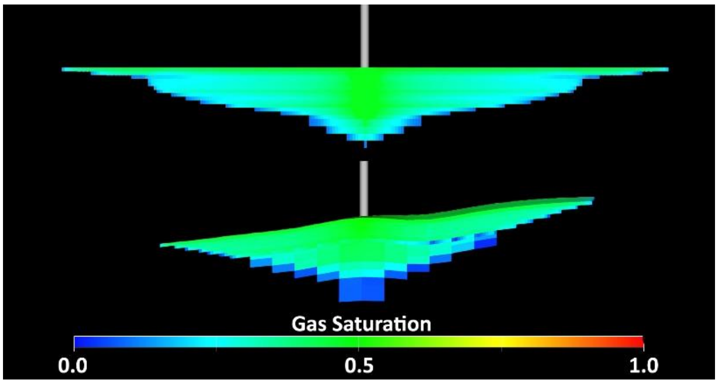

Figure 11. The effect of storage complex structure on injected CO_2 migration.

3.4 Comparison of analytical and numerical results

The base case horizontal migration distance is also calculated analytically (Nordbotten et al. 2005), using the dimensionless parameter $\boldsymbol{\Gamma}$ = 0.5 as calculated using the injection rate. These results are compared to base case horizontal migration distances from the numerical simulation (Figure 12), except that the injection zone is made homogeneous to more accurately resemble the analytical calculation.

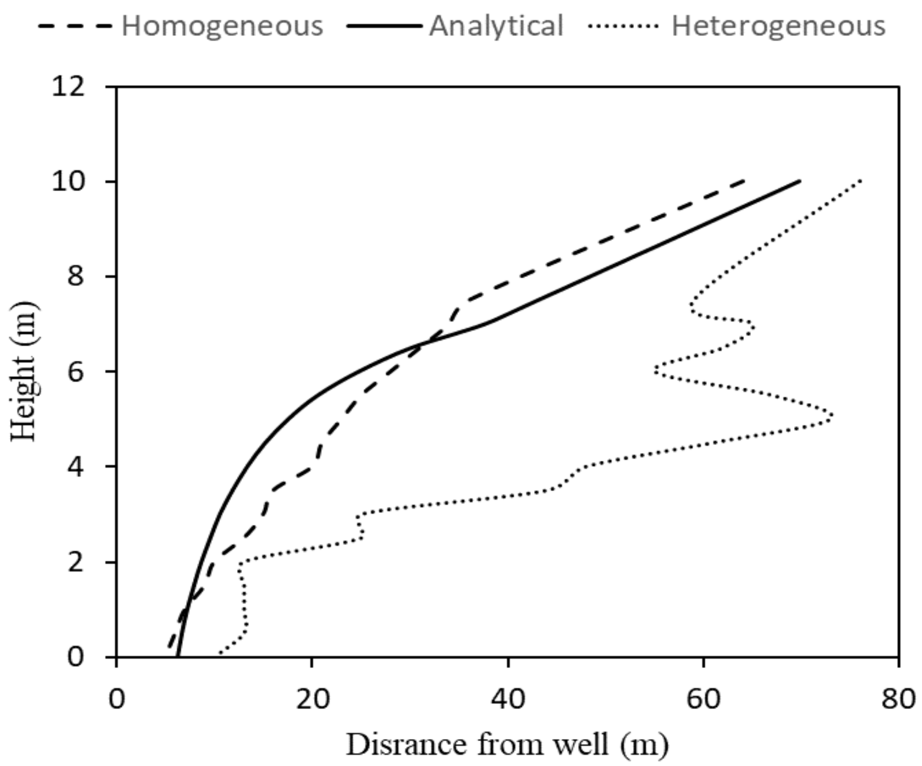

Figure 12. Comparison of the migration distance for the analytical solution and homogenous and heterogeneous numerical simulation at the FRS

The comparison shows that the results of the analytical solution are generally consistent with the homogeneous and isotropic numerical model (Figure 12).

It can also be seen in Figure 12 that the migration plume obtained for the homogeneous case is overall higher than that for the heterogeneous case. It is obvious that the reservoir heterogeneity inhibits the vertical plume migration. However, the heterogeneity can enhance the lateral movement, as is shown in Figure 12 that the horizontal migration distance is 74 m in the heterogeneous model but only 62 m in the homogeneous model. Overall, reservoir heterogeneity can also have an important influence on CO_2 plume migration, which is also found by Al- Khdheeawi et al. (2017).

4. Conclusion

The simulated CO_2 plume horizontal extent, vertical saturation distribution, and dissolution rate at the FRS are studied by conducting a sensitivity analysis of selected model parameters. The effects of variations in the k_v/k_h ratio, horizontal permeability, and the injection rate are investigated. From the model results we conclude:

1. The effect of k_v/k_h ratios on vertical and horizontal migration is not apparent at the start of injection but their effects become more significant with increasing time. With a higher k_v/k_h ratio, both vertical and horizontal migration distances increase. Higher model k_v/k_h ratios predict a lower dissolution rate and a lower total amount of dissolved CO_2.
2. Higher horizontal permeability enhances the vertical migration rate initially, although this effect declines over time. Models with high horizontal permeability trap a proportion of injected CO_2 in the upper reservoir layers. CO_2 horizontal migration is facilitated by increased horizontal permeability. Models outcomes with higher horizontal permeability also exhibit almost one order of magnitude increased dissolved CO_2.
3. In all cases, the cumulative CO_2 injected is identical (i.e. the injection interval is shorter for models with higher injection rates), vertical migration extent is not dependent on injection rate, largely due to model architecture, but horizontal migration is larger when injection rates are lower, probably due to a more even distribution of CO_2 throughout the reservoir. Higher CO_2 injection rates are also

associated with slightly decreased model dissolution rates and decreased cumulative dissolved CO_2.

4. Our results suggest that CCS project CO_2 injection rate should be carefully determined considering the results of reservoir models.
5. The analytical analysis provides a useful method for confirming migration distances obtained from numerical simulation, where an assumption of injection zone homogeneity is reasonable.
6. The reservoir heterogeneity can enhance the lateral movement while inhibits the vertical plume migration during the injection interval.

5. Future work

Although this study is based on the FRS, some conclusions are more generally applicable to other CO_2 storage sites. Model sensitivity to the relative permeability curve, capillary pressure merit further study. Having predicted the time of arrival and shape of the plume at the FRS, the next step is to compare and analyze model predictions against the observed arrival of injected CO_2 at the observation wells and the various images of the plume when that occurs to better understand the conformance of model and observed results.

6. Acknowledgments

The authors thank the Centre for Fluid and Complex Systems for the financial support of this project. We thank the Containment and Monitoring Institute (CaMI) of CMC Research Institutes Inc. for providing the geostatic model and petrophysical data for the FRS. Research at the site is undertaken thanks in part to funding from the Canada First Research Excellence Fund. Special thanks also to Dr. Phil Costen for reviewing the paper and sharing his constructive comments.

Appendix: Analytical solution of CO_2 plume

The CO_2 plume analytical solution is Nordbotten et al. (2005)

$$-\frac{\lambda-1}{r'\left((\lambda-1)b'+1\right)^2} + 2\Gamma r'b' + 2\Lambda r' = 0, \tag{1}$$

$$\Lambda(\lambda-1)^2 - \Gamma\lambda \ln\left(\frac{\Gamma+\Lambda}{\Lambda\lambda}\right) = \frac{2\lambda[\Lambda(\lambda-1)-\Gamma]^2}{\lambda-1}. \tag{2}$$

where $\boldsymbol{\lambda}$ is the averaged phase mobility of water and CO_2, defined as $\boldsymbol{\lambda} = \frac{b}{B}\lambda_c + \frac{B-b}{B}\lambda_w$, and b denotes the thickness of the CO_2 layer, and B represents the total reservoir thickness. $\lambda_\alpha = \frac{k_{r\alpha}}{\mu_\alpha}$, is the ratio of relative permeability to fluid viscosity, where $\boldsymbol{\alpha}$ represents each phase, with c for CO_2 and w for water. $\boldsymbol{\Lambda}$ denotes the Lagrangian multiplier.

In addition, $\boldsymbol{r'}$, $\boldsymbol{b'}$ and $\boldsymbol{\Gamma}$are dimensionless variables, where $r' = r\sqrt{\frac{\pi B\varphi}{Q_{well}t}}$, $b' = \frac{b}{B}$, and $\Gamma = \frac{2\pi\Delta\rho g\lambda_w kB^2}{Q_{well}}$. In these equations, r denotes migration distance, $\boldsymbol{\Delta\rho}$ is the density differential between brine and CO_2, g is the gravitational constant, k is the average permeability of the reservoir, $\boldsymbol{\varphi}$ is the average porosity, t is the injection period and $\boldsymbol{Q_{well}}$ is the CO_2 injection rate. For simplicity, water and CO_2 viscosities and densities are assumed constant. Fluid properties of CO_2 and brine used in these calculations are shown in Table 1.

References

Ahmadinia, M., Shariatipour, S. M., Andersen, O., & Sadri, M. (2019). Benchmarking of vertically integrated models for the study of the impact of caprock morphology on CO_2 migration. *International Journal of Greenhouse Gas Control*, *90*(August), 102802. https://doi.org/10.1016/j.ijggc.2019.102802

Al-Khdheeawi, E. A., Vialle, S., Barifcani, A., Sarmadivaleh, M., & Iglauer, S. (2017). Impact of reservoir wettability and heterogeneity on CO_2-plume migration and trapping capacity. *International Journal of Greenhouse Gas Control*, *58*, 142–158. https://doi.org/10.1016/j.ijggc.2017.01.012

Arts, R., Eiken, O., Chadwick, A., Zweigel, P., van der Meer, L., & Zinszner, B. (2004). Monitoring of CO_2 injected at Sleipner using time-lapse seismic data. *Energy*, *29*(9–10), 1383–1392. https://doi.org/10.1016/j.energy.2004.03.072

Bachu, S. (2008). CO_2 storage in geological media: Role, means, status and barriers to deployment. *Progress in Energy and Combustion Science*, *34*(2), 254–273. https://doi.org/10.1016/j.pecs.2007.10.001

Bergmo, P. E. S., Grimstad, A. A., & Lindeberg, E. (2011). Simultaneous CO_2 injection and water production to optimise aquifer storage capacity. *International Journal of Greenhouse Gas Control*, *5*(3), 555–564. https://doi.org/10.1016/j.ijggc.2010.09.002

Birkholzer, J. T., Cihan, A., & Zhou, Q. (2012). Impact-driven pressure management via targeted brine extraction-Conceptual studies of CO_2 storage in saline formations. *International Journal of Greenhouse Gas Control*, *7*, 168–180. https://doi.org/10.1016/j.ijggc.2012.01.001

Birkholzer, J. T., Oldenburg, C. M., & Zhou, Q. (2015). CO_2 migration and pressure evolution in deep saline aquifers. *International Journal of Greenhouse Gas Control*, *40*, 203–220. https://doi.org/10.1016/j.ijggc.2015.03.022

Birkholzer, J. T., & Zhou, Q. (2009). Basin-scale hydrogeologic impacts of CO_2 storage: Capacity and regulatory implications. *International Journal of Greenhouse Gas Control*, *3*(6), 745–756. https://doi.org/10.1016/j.ijggc.2009.07.002

Brooks, R., & Corey, T. (1964). HYDRAU uc properties of porous media. *Hydrology Papers, Colorado State University*, *24*, 37.

Bryant, S. L., Lakshminarasimhan, S., & Pope, G. A. (2006). SPE 99938 Buoyancy - Dominated Multiphase Flow and Its Impact on Geological Sequestration. *SPE Journal*.

Buscheck, T. A., Sun, Y., Chen, M., Hao, Y., Wolery, T. J., Bourcier, W. L., et al. (2012). Active CO_2 reservoir management for carbon storage: Analysis of operational strategies to relieve pressure buildup and improve injectivity. *International Journal of Greenhouse Gas Control*, *6*, 230–245. https://doi.org/10.1016/j.ijggc.2011.11.007

Carroll, S., Hao, Y., & Aines, R. (2009). Transport and detection of carbon dioxide in dilute aquifers. *Energy Procedia*, *1*(1), 2111–2118. https://doi.org/10.1016/j.egypro.2009.01.275

Chang, Y.-B., Coats, B. K., & Nolen, J. S. (1996). A compositional model for CO_2 floods including CO_2 solubility in water. In *Permian Basin Oil and Gas Recovery Conference*. Society of Petroleum Engineers.

Chasset, C., Jarsjö, J., Erlström, M., Cvetkovic, V., & Destouni, G. (2011). Scenario simulations of CO_2 injection feasibility, plume migration and storage in a saline aquifer, Scania, Sweden. *International Journal of Greenhouse Gas Control*, *5*(5), 1303–1318. https://doi.org/10.1016/j.ijggc.2011.06.003

Cihan, A., Birkholzer, J. T., & Bianchi, M. (2015). Optimal well placement and brine extraction for pressure management during CO_2 sequestration. *International Journal of Greenhouse Gas Control*, *42*, 175–187.

https://doi.org/10.1016/j.ijggc.2015.07.025

Daley, T. M., Solbau, R. D., Ajo-Franklin, J. B., & Benson, S. M. (2007). Continuous crosswell monitoring of CO_2 injection in a brine aquifer. *Society of Exploration Geophysicists - 77th SEG International Exposition and Annual Meeting, SEG 2007*, *72*(5), 2949–2953. https://doi.org/10.1190/1.2793083

Dempsey, D., Kelkar, S., & Pawar, R. (2014). Passive injection: A strategy for mitigating reservoir pressurization, induced seismicity and brine migration in geologic CO_2 storage. *International Journal of Greenhouse Gas Control*, *28*, 96–113. https://doi.org/10.1016/j.ijggc.2014.06.002

Dongas, J. M., & Lawton, D. C. (2016). Static characterization and dynamic simulated scenarios for monitoring a shallow CO_2 injection target, (Figure 1), 2–6. https://www.crewes.org/ForOurSponsors/ConferenceAbstracts/2016/CSEG/Dongas_CSEG_2016.pdf

Doughty, C. (2010). Investigation of CO_2 plume behavior for a large-scale pilot test of geologic carbon storage in a saline formation. *Transport in Porous Media*, *82*(1), 49–76. https://doi.org/10.1007/s11242-009-9396-z

Flett, M., Gurton, R., & Weir, G. (2007). Heterogeneous saline formations for carbon dioxide disposal: Impact of varying heterogeneity on containment and trapping. *Journal of Petroleum Science and Engineering*, *57*(1–2), 106–118. https://doi.org/10.1016/j.petrol.2006.08.016

Han, W. S., Lee, S.-Y., Lu, C., & McPherson, B. J. (2010). Effects of permeability on CO_2 trapping mechanisms and buoyancy-driven CO_2 migration in saline formations . *Water Resources Research*, *46*(7), 1–20. https://doi.org/10.1029/2009wr007850

Hesse, M. A., & Woods, A. W. (2010). Buoyant dispersal of CO_2 during geological storage. *Geophysical Research Letters*, *37*(1), 1–5. https://doi.org/10.1029/2009GL041128

Hovorka, S. D., Doughty, C., Benson, S. M., Pruess, K., & Knox, P. R. (2004). The impact of geological heterogeneity on CO_2 storage in brine formations: A case study from the Texas Gulf Coast. *Geological Society Special Publication*, *233*, 147–163. https://doi.org/10.1144/GSL.SP.2004.233.01.10

IEA. (2013). Technology Roadmap Carbon Capture and Storage–2013 Edition. Organization for Economic Co-operation and Development/International Energy.

Juanes, R., MacMinn, C. W., & Szulczewski, M. L. (2010). The footprint of the CO_2 plume during carbon dioxide storage in saline aquifers: Storage efficiency for capillary trapping at the basin scale. *Transport in Porous Media*, *82*(1), 19–30. https://doi.org/10.1007/s11242-009-9420-3

Lawton, D. C., Dongas, J., Osadetz, K., Saeedfar, A., & Macquet, M. (2019). Development and analysis of a geostatic model for shallow CO_2 injection at the Field Research Station, Southern Alberta, Canada. *Geophysics and*

Geosequestration. Cambridge University Press, Cambridge, *280*, 296.

Lawton, D. C., Osadetz, K. G., & Saeedfar, A. (2017). CCS monitoring technology innovation at the CaMI Field research station, Alberta, Canada. *EAGE/SEG Research Workshop 2017 on Geophysical Monitoring of CO_2 Injections: CCS and CO_2-EOR*, (Mmv), 5–9. https://doi.org/10.3997/2214-4609.201701930

Li, B., & Benson, S. M. (2015). Influence of small-scale heterogeneity on upward CO_2 plume migration in storage aquifers. *Advances in Water Resources*, *83*, 389–404. https://doi.org/10.1016/j.advwatres.2015.07.010

Li, K., & Horne, R. N. (2006). Comparison of methods to calculate relative permeability from capillary pressure in consolidated water-wet porous media. *Water Resources Research*, *42*(6), 1–9. https://doi.org/10.1029/2005WR004482

Macquet, M., Lawton, D. C., Saeedfar, A., & Osadetz, K. G. (2019). A feasibility study for detection thresholds of CO_2 at shallow depths at the CaMI Field Research Station, Newell County, Alberta, Canada . *Petroleum Geoscience*, *25*, petgeo2018-135. https://doi.org/10.1144/petgeo2018-135

Metz, B. (2005). carbon dioxide capture and storage. *IPCC special report*, 342.

Morris, J. P., Detwiler, R. L., Friedmann, S. J., Vorobiev, O. Y., & Hao, Y. (2011). The large-scale geomechanical and hydrogeological effects of multiple CO_2 injection sites on formation stability. *International Journal of Greenhouse Gas Control*, *5*(1), 69–74. https://doi.org/10.1016/j.ijggc.2010.07.006

Newell, A. J., Pourmalek, A., Butcher, A. S., & Shariatipour, S. M. (2019). The importance of lithofacies control on fluid migration in heterogeneous aeolian formations for geological CO_2 storage: Lessons from observational evidence and modelling of bleached palaeoreservoirs at Salt Wash Graben, Utah. *International Journal of Greenhouse Gas Control*, *91*(September), 102841. https://doi.org/10.1016/j.ijggc.2019.102841

Nordbotten, J. M., Celia, M. A., & Bachu, S. (2005). Injection and storage of CO_2 in deep saline aquifers: Analytical solution for CO_2 plume evolution during injection. *Transport in Porous Media*, *58*(3), 339–360. https://doi.org/10.1007/s11242-004-0670-9

Onoja, M. U., Ahmadinia, M., Shariatipour, S. M., & Wood, A. M. (2019). Characterising the role of parametric functions in the van Genuchten empirical model on CO_2 storage performance. *International Journal of Greenhouse Gas Control*, *88*(June), 233–250. https://doi.org/10.1016/j.ijggc.2019.06.004

Onoja, M. U., & Shariatipour, S. M. (2019). Assessing the impact of relative permeability and capillary heterogeneity on Darcy flow modelling of CO_2 storage in Utsira Formation. *Greenhouse Gases: Science and Technology*, *26*(2019), 1–26. https://doi.org/10.1002/ghg.1932

Rock, L., O'Brien, S., Tessarolo, S., Duer, J., Bacci, V. O., Hirst, B., et al. (2017). The Quest CCS Project: 1st Year Review Post Start of Injection. *Energy Procedia*, *114*(November 2016), 5320–5328.

https://doi.org/10.1016/j.egypro.2017.03.1654

Rutqvist, J., Birkholzer, J., Cappa, F., & Tsang, C. F. (2007). Estimating maximum sustainable injection pressure during geological sequestration of CO_2 using coupled fluid flow and geomechanical fault-slip analysis. *Energy Conversion and Management*, *48*(6), 1798–1807. https://doi.org/10.1016/j.enconman.2007.01.021

Shariatipour, S. M., Mackay, E. J., & Pickup, G. E. (2016). An engineering solution for CO_2 injection in saline aquifers. *International Journal of Greenhouse Gas Control*, *53*, 98–105. https://doi.org/10.1016/j.ijggc.2016.06.006

Shariatipour, S. M., Pickup, G. E., & Mackay, E. J. (2016a). Investigation of CO_2 storage in a saline formation with an angular unconformity at the caprock interface. *Petroleum Geoscience*, *22*(2), 203–210. https://doi.org/10.1144/petgeo2015-039

Shariatipour, S. M., Pickup, G. E., & Mackay, E. J. (2016b). Simulations of CO_2 storage in aquifer models with top surface morphology and transition zones. *International Journal of Greenhouse Gas Control*, *54*, 117–128. https://doi.org/10.1016/j.ijggc.2016.06.016

Taku Ide, S., Jessen, K., & Orr, F. M. (2007). Storage of CO_2 in saline aquifers: Effects of gravity, viscous, and capillary forces on amount and timing of trapping. *International Journal of Greenhouse Gas Control*, *1*(4), 481–491. https://doi.org/10.1016/S1750-5836(07)00091-6

Tucker, O., Gray, L., Maas, W., Solutions, S. G., Brien, S. O., & Canada, S. (2016). IPTC-18666-MS Quest Commercial Scale CCS – The First Year Overview of the Quest CCS project, (November), 14–16.

UNCCS. (2015). Climate Action Now: Summary for Policymakers 2015.

Yang, F., Bai, B., Dunn-Norman, S., Nygaard, R., & Eckert, A. (2014). Factors affecting CO_2 storage capacity and efficiency with water withdrawal in shallow saline aquifers. *Environmental Earth Sciences*, *71*(1), 267–275. https://doi.org/10.1007/s12665-013-2430-z

Zakirov, I., I. Aanonsen, S., S. Zakirov, E., & M. Palatnik, B. (2014). Optimizing Reservoir Performance by Automatic Allocation of Well Rates. *ECMOR V - 5th European Conference on the Mathematics of Oil Recovery*, 375–384. https://doi.org/10.3997/2214-4609.201406895

Zatsepina, O. Y., Hassanzadeh, H., & Pooladi-Darvish, M. (2014). Geological Storage of CO_2 as Hydrate in a McMurray Depleted Gas Reservoir. *Gas Injection for Disposal and Enhanced Recovery*, *9781118938*(September), 311–329. https://doi.org/10.1002/9781118938607.ch18

Zhou, Q., Birkholzer, J. T., Mehnert, E., Lin, Y. F., & Zhang, K. (2010). Modeling basin- and plume-scale processes of CO_2 storage for full-scale deployment. *Ground Water*, *48*(4), 494–514. https://doi.org/10.1111/j.1745-6584.2009.00657.x

716